ACS APPLIED MATERIALS & INTERFACES

Research Article

www.acsami.org

Integrated Trilayered Silk Fibroin Scaffold for Osteochondral Differentiation of Adipose-Derived Stem Cells

Xiaoming Ding,[†,§,⊥] Meifeng Zhu,[‡,⊥] Baoshan Xu,[†] Jiamin Zhang,[‡] Yanhong Zhao,[∥] Shenglu Ji,[‡] Lina Wang,[‡] Lianyong Wang,[*,‡] Xiulan Li,[†] Deling Kong,[‡] Xinlong Ma,[†] and Qiang Yang[*,†]

[†]Department of Spine Surgery, Tianjin Hospital, Tianjin 300211, People's Republic of China

[‡]Key Laboratory of Bioactive Materials, Ministry of Education, College of Life Sciences, Nankai University, Tianjin 300071, People's Republic of China

[§]Tianjin Medical University, Tianjin 300070, People's Republic of China

[∥]Stomatological Hospital of Tianjin Medical University, Tianjin 300070, People's Republic of China

Supporting Information

ABSTRACT: Repairing osteochondral defects (OCD) remains a formidable challenge due to the high complexity of native osteochondral tissue and the limited self-repair capability of cartilage. Osteochondral tissue engineering is a promising strategy for the treatment of OCD. In this study, we fabricated a novel integrated trilayered scaffold using silk fibroin and hydroxyapatite by combining paraffin-sphere leaching with a modified temperature gradient-guided thermal-induced phase separation (TIPS) technique. This biomimetic scaffold is characterized by three layers: a chondral layer with a longitudinally oriented microtubular structure, a bony layer with a 3D porous structure and an intermediate layer with a dense structure. Live/dead and CCK-8 tests indicated that this scaffold possesses good biocompatibility for supporting the growth, proliferation, and infiltration of adipose-derived stem cells (ADSCs). Histological and immunohistochemical stainings and real-time polymerase chain reaction (RT-PCR) confirmed that the ADSCs could be induced to differentiate toward chondrocytes or osteoblasts in vitro at chondral and bony layers in the presence of chondrogenic- or osteogenic-induced culture medium, respectively. Moreover, the intermediate layer could play an isolating role for preventing the cells within the chondral and bony layers from mixing with each other. In conclusion, the trilayered and integrated osteochondral scaffolds can effectively support cartilage and bone tissue generation in vitro and are potentially applicable for OC tissue engineering in vivo.

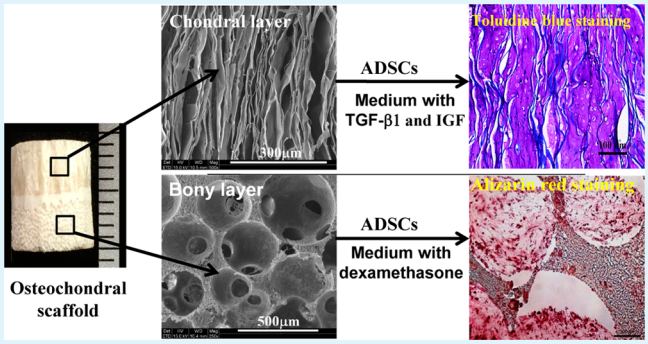

KEYWORDS: *osteochondral tissue engineering, calcified cartilage layer, adipose-derived stem cells, silk fibroin, integrated scaffold*

1. INTRODUCTION

Osteochondral defects (OCD) resulting from trauma, tumor resection, or osteoarthritis are common orthopedic diseases. The current treatment strategies, including debridement, bone-marrow stimulation, and total joint arthroplasty, have shown limited healing capacity for these defects.[1,2] Debridement and bone-marrow stimulation are only palliative and are not completely curative. Total joint arthroplasty features an immune rejection response and disease transmission.[2] Repairing OCD remains a formidable challenge because of the high complexity of native osteochondral tissue and the limited self-repair capability of cartilage.[3,4] The emergence of tissue engineering has provided a promising alternative therapy for the treatment of OCD.[5−7]

For osteochondral tissue engineering, the selection of biomaterials, design of the scaffold structure, and methods of fabrication are crucial for successful development of suitable scaffolds, which should closely mimic the native physiological structure and environment of osteochondral tissue.[1,2,5−7] On the basis of the native osteochondral physiological structure, many researchers have designed and fabricated bilayered scaffolds with a chondral layer and a bony layer for simultaneously regenerating both cartilage and subchondral bone.[6] However, these bilayered scaffolds were integrated by suturing or adhering the separate chondral and bony layers before or after seeding cells, which could result in unsatisfactory regeneration of OCD.[8−10] In addition, most of the bilayered scaffolds were not designed to incorporate an intermediate layer between the chondral and bony layers. The intermediate layer is expected to develop into a calcified cartilage layer between the cartilage and subchondral bone. The calcified cartilage layer serves as a vital physical barrier for the formation

Received: June 10, 2014
Accepted: September 11, 2014
Published: September 11, 2014

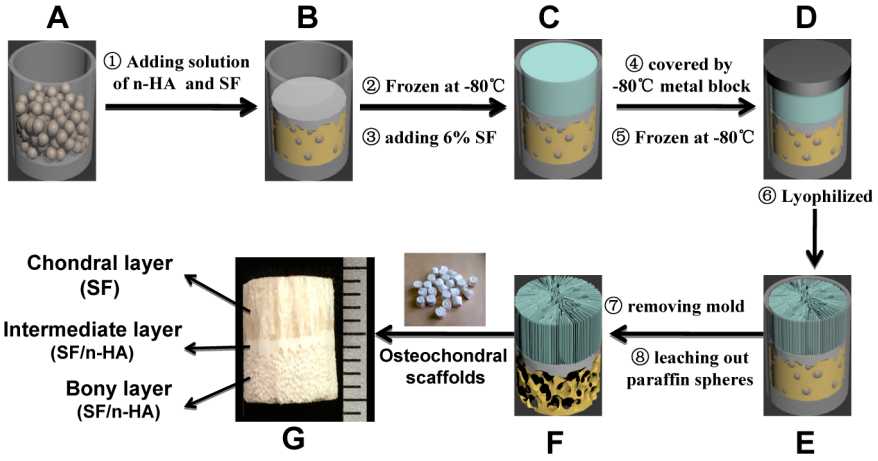

Figure 1. (A–F) Schematic diagrams of the process for preparing integrated osteochondral scaffolds. (G) Gross appearance of scaffold.

of cartilage and bone in different environments of oxygen and nutrients. Without this calcified cartilage layer, the formation of new cartilage and osteochondral tissue will be impaired;[11−14] therefore, the calcified cartilage layer is considered to be a prerequisite for functional and integrative repair of osteochondral tissue. To create a calcified cartilage layer and to closely mimic the native osteochondral structure and regeneration environment, a trilayered scaffold that contains an intermediate layer, a chondral layer, and a bony layer was proposed for the simultaneous regeneration of cartilage, calcified cartilage, and bone.[15,16] However, developing a simple and efficient approach for fabricating a trilayered osteochondral scaffold that contains an intermediate layer that can be tightly bonded with the chondral and bony layers remains a challenge.

Primary chondrocytes and osteoblasts are the most direct sources of cells for osteochondral tissue engineering.[17] However, these cells have disadvantages with respect to their limited numbers of cells and dedifferentiation,[18] which restrict their application in osteochondral tissue engineering. Stem cells are an alternative resource for overcoming these limitations. Specifically, bone marrow mesenchymal stem cells (MSCs) are widely used because of their ability to differentiate into chondrocytes and osteoblasts.[19,20] Recently, researchers have confirmed that the biology and differentiation potential of adipose-derived stromal cells (ADSCs) are similar to those of MSCs and that ADSCs could also be induced to differentiate into chondrocytes and osteoblasts under appropriate conditions.[21,22] ADSCs can be obtained from autologous fat tissue with minimal injury and with large yields.[23,24] Currently, increasing numbers of studies are applying ADSCs in osteochondral tissue engineering and in other fields of regenerative medicine.[25,26]

Silk fibroin (SF), which is a natural biomaterial, has many outstanding characteristics, such as good biocompatibility, proper mechanical properties, low immunogenicity, and a controllable degradation rate.[27,28] SF materials are promising candidates for fabricating bone and chondrocyte scaffolds.[29−31] Hydroxyapatite (HA) is the major mineral constituent of the bone matrix. Combining natural or synthetic polymers such as poly(lactic-*co*-glycolic acid) (PLGA),[32] chitosan,[33] collagen,[34] and SF[35] with HA is a promising strategy for creating bone scaffolds because of the bioactivity and osteoconductivity of HA.

In the present study, we developed a novel integrated osteochondral scaffold by combining paraffin-sphere leaching with a directional crystallization technique. The osteochondral scaffold contains three layers: the upper layer is a longitudinally oriented structure of SF that mimics native cartilage, the lower layer is a 3D porous structure composed of SF and HA that mimics subchondral bone, and the dense intermediate layer is also composed of SF and HA and serves as the boundary between the chondral and bony layers and enhances the integrated strength of the complete scaffold. We evaluated the adhesion, proliferation, and differentiation of chondrogenic- and osteogenic-induced ADSCs on this scaffold in vitro.

2. EXPERIMENTAL SECTION

2.1. Materials. *Bombyx mori* silkworm silk was purchased from Suzhou, China. SF solution was prepared as previously described.[36] HA was obtained from Nanjing Aipurui Nano Material (China). Other materials, including biochemical and chemical reagents, are listed in Supporting Information.

2.2. Fabrication and Characterization of Scaffolds. *2.2.1. Scaffold Fabrication.* The integrated osteochondral scaffold was prepared by a stratified strategy that combined paraffin sphere leaching with a modified temperature gradient-guided thermal-induced phase separation (TIPS) technique. First, paraffin spheres with diameters of 350–425 μm were added to a Teflon mold (Figure 1A). The surface of the paraffin spheres was leveled by use of a flat-head metal block with proper pressure. The mold filled with paraffin spheres was carefully placed in a preheated oven at 50 °C for 60 min, and then it was cooled to room temperature, thereby creating a paraffin sphere assembly. HA and SF were mixed at an equivalent weight ratio and then added to the paraffin sphere assembly under vacuum such that the mixture could fill all of the spaces between the paraffin spheres. Most of the excess mixture was removed, and only a small amount of the mixture remained as a thin layer covering the top surface of the paraffin sphere assembly (Figure 1B). The mold was frozen at −80 °C and then briefly placed at room temperature to slightly melt the surface of the thin layer. Next, the SF solution (6 wt %) was added to fill the entire mold (Figure 1C), which was then covered with a precooled metal block at −80 °C (Figure 1D) for approximately 15 min. The mold covered with the metal block was placed in a −80 °C refrigerator for 4 h. The integrated trilayer composite was obtained by freeze-drying (Figure 1E). The composite was soaked in 90% (v/v) methanol for 2 h to induce the crystallization of SF. The paraffin spheres in the composite were extracted with hexane to obtain an integrated trilayer porous scaffold that contained the chondral, intermediate, and bony layers (Figure 1F,G).

2.2.2. Characterization of Integrated Osteochondral Scaffolds. The resulting integrated osteochondral scaffolds were characterized by scanning electron microscopy (SEM), micro computed tomography (micro-CT), X-ray diffraction (XRD), and Fourier transform infrared

(FTIR) spectroscopy. Briefly, the scaffold specimens were cut into longitudinal sections of integrated scaffold and into cross sections of the top layer and bottom layer with a scalpel blade. All sections were examined by SEM (Quanta 200, FEI) after being coated with gold–palladium. Average pore sizes of the chondral and bony layers were determined by measuring >50 random pores with sizes larger than 20 μm, which were selected from the SEM images by use of ImageJ (U.S. National Institutes of Health). The truncated cylindrical integrated scaffold was soaked in 2% osmic acid for 48 h and freeze-dried, and then it was examined by micro-CT (Sky Scan 1174, Belgium). Structural parameters of the scaffolds, such as total examined scaffold volume (TV) and scaffold volume (SV), were obtained from the micro-CT measurements. Scaffold volume density could be calculated as SV/TV, and the scaffold porosity was defined as $(1 - SV/TV) \times 100$.

FTIR spectra of the scaffolds were recorded between 400 and 2500 cm^{-1} on a FTIR spectrometer (PerkinElmer 1600). For each spectrum, 64 scans were acquired at 4 cm^{-1} resolution.

XRD patterns of the scaffolds were recorded on an X-ray diffractometer (D/max 2500, Japan) with Cu Kα radiation. The voltage of the X-ray source was 30 kV at 30 mA, and the scan speed was 8°/min.

2.3. Isolation and Culture of Adipose-Derived Stromal Cells. ADSCs were isolated from 4-month-old New Zealand rabbits as previously described.[23,24] All of the experimental protocols were approved by the Animal Experimental Ethics Committee of Tianjin Hospital. Briefly, adipose tissue derived from subcutaneous tissue of the necks of the rabbits was harvested and thoroughly washed three times with a phosphate-buffered saline (PBS) solution containing 10% penicillin/streptomycin. Then visible blood vessels and connective tissue were removed. The cleaned adipose tissue was digested with 0.1% type I collagenase at 37 °C for 1 h. To counteract the type I collagenase activity, 5 mL of Dulbecco's modified Eagle medium (DMEM) containing 10% fetal bovine serum (FBS) was added. The obtained tissue homogenate was centrifuged at 300*g*, the supernate was removed along with the mature adipocytes, and the ADSCs were left as residue. The resulting ADSC pellet was resuspended in DMEM that contained 20% FBS and 1% penicillin/streptomycin and then cultured in flasks in a 5% CO_2 humidified incubator at 37 °C. Nonadherent cells were removed by changing the medium, and the adherent cells were expanded to passage 3. To characterize the obtained ADSCs, the ADSCs were stained with phycoerythrin (PE)-conjugated anti-rabbit monoclonal antibodies (CD44-PE, CD105-PE, and CD34-PE) (Bioss, Beijing, China) to examine the expression of CD44, CD105, and CD34 by flow cytometry (Becton Dickinson); the results are shown in Figure S1 in Supporting Information.

2.4. Adipose-Derived Stromal Cell Culture in Chondrogenic or Osteogenic Induction Medium. ADSCs were cultured in chondrogenic or osteogenic induction medium, which allowed an adequate number of cells to be obtained. Briefly, the ADSCs were divided into two groups. The first group for osteogenic induction was cultured in osteogenic induction medium that contained 0.1 μM dexamethasone, 10 mM β-glycerol phosphate, 50 μM ascorbate 2-phosphate, 10% FBS, and 1% penicillin/streptomycin. The second group for chondrogenic induction was cultured in chondrogenic induction medium that contained 10 ng/mL transforming growth factor β1 (TGF-β1), 100 ng/mL insulin-like growth factor 1 (IGF-1), 50 μg/mL ascorbate 2-phosphate, 40 μg/mL L-proline, ITS (6.25 μg/mL insulin, 6.25 μg/mL transferrin, and 6.25 ng/mL selenous acid), 10% FBS, 100 μg/mL pyruvate, and 300 μg/mL L-glutamine. After 7 days of culturing, in which the medium was changed every 2 days, chondrogenic- and osteogenic-induced ADSCs were obtained.[37]

2.5. Adhesion and Viability of Induced Adipose-Derived Stromal Cells. To evaluate the adhesion of induced ADSCs on the integrated osteochondral scaffold, 25 μL of a suspension containing 2.5×10^5 chondrogenic-induced ADSCs was first seeded onto the chondral layer of the cylindrical integrated scaffolds (diameter of 5 mm with a 1.5 mm thick chondral layer and 3 mm thick bony layer) and incubated for 2 h, and then 1 mL of medium was added. After 1 day of culturing, the scaffold with the chondrogenic-induced ADSCs was inverted, 50 μL of a suspension containing 5×10^5 osteogenic-induced ADSCs was seeded onto the bony layer and incubated for 2 h, and then 1 mL of medium was added. After an additional 7 days of culturing, the cylindrical integrated scaffolds with cells were fixed with 2.5% glutaraldehyde for 4 h and then dehydrated through a graded series of ethanol. The dried scaffolds were cut into longitudinal sections with a thickness of 1 mm and coated with gold. The adhesion of induced ADSCs on each layer of the integrated scaffold was observed by SEM.

The viability of the induced ADSCs within the integrated scaffold was assessed by use of a live/dead cell viability assay kit after 7 days of culturing. After incubation with the live/dead staining solution for 30 min, the cell-seeded scaffolds were gently rinsed in sterilized PBS, and live cells (green) and dead cells (red) were observed by confocal microscopy (Leica).

2.6. Assessment of Isolating Role of the Intermediate Layer. To confirm that the intermediate layer served as an isolation layer, we seeded DiO-labeled ADSCs (DiO, green fluorescent dye, Sigma) and DiI-labeled ADSCs (DiI, red fluorescent dye, Sigma) onto the chondral and bony layers, respectively. After 7 days of culturing, the labeled ADSC scaffold composite was cut into longitudinal sections of thickness 150 μm. The sections were stained with 4′,6-diamidino-2-phenylindole (DAPI, Sigma) and then directly observed under a confocal microscope (Leica).

2.7. Histological and Immunohistological Analysis. Differentiation of induced ADSCs and deposition of extracellular matrix (ECM) were evaluated by histological and immunohistological analysis. Briefly, chondrogenic- and osteogenic-induced ADSCs were seeded onto the chondral and bony layers, respectively, and were cultured in chondrogenic or osteogenic induction medium for 7 and 21 days. Then the cells were fixed with 10% formalin, dehydrated, paraffin-embedded, and cut into sections with thicknesses of 7 μm. The sections were deparaffinized, rehydrated and stained with hematoxylin and eosin (H/E) (Sigma–Aldrich, St. Louis, MO) to observe the distribution of cells. The sections of chondral layers were stained with toluidine blue and safranin O to evaluate glycosaminoglycan (GAG). The sections of osteogenic layers were stained with alizarin red and von Kossa to determine the deposition of calcium. For immunohistochemistry, collagen type II in the chondral layers and collagen type I in the bony layers were detected using a kit. Briefly, deparaffinized and rehydrated sections were incubated for 10 min with a 3% peroxidase solution, blocked with a 5% bovine serum albumin (BSA) solution for 20 min, incubated with the primary antibodies (rabbit anti-collagen II and I) at 4 °C overnight, and then washed and incubated with biotinylated secondary antibody for 20 min. The treated sections were incubated with streptavidin–biotin complex (SABC) for 20 min at 37 °C and then developed with diaminobenzidine (DAB) and observed by inverted light microscopy (Leica).

2.8. Quantitative Analysis of Cell Proliferation and Extracellular Matrix. Chondrogenic- and osteogenic-induced ADSCs were seeded onto the separated chondral and bony layers, respectively, and were cultured for 1, 7, and 21 days. Cell proliferation was quantified by use of a cell counting kit (CCK-8). Briefly, at each time point, cell-scaffold samples (n = 5) were harvested, rinsed in PBS, and then incubated with 100 μL of fresh serum-free DMEM medium that contained 10% CCK-8 solution at 37 °C under 5% CO_2 for 3 h. Optical density (OD) was measured at 450 nm on a microplate reader (iMark, Bio-Rad, Japan). Fresh serum-free DMEM with 10% CCK-8 was used as a control.

The chondrogenic matrix, including glycosaminoglycan (GAG) and collagen II in the chondral layer, was quantified. Briefly, the cell-scaffold samples (n = 5) were rinsed in PBS, minced, and homogenized in PBS by use of a glass grinder. The resulting suspensions were subjected to two freeze–thaw cycles to further break the cell membranes. Then the homogenates were centrifuged for 15 min at 5000 rpm, after which the supernatants were immediately removed. The contents of GAG and collagen type II were measured by use of a rabbit GAG enzyme-linked immunosorbent assay (ELISA) kit and a collagen type II ELISA kit (Blue Gene Biotech, Shanghai)

Table 1. RT-PCR Primer Sequences

gene	primer sequences	
	forward	reverse
GAPDH	GACTGATGTTGTTGACAGCCACTGC	TAGCCACTCCTTCTGTGACTCTAAC
collagen II	CACCACGCTCTTCTGTCTACTGAAC	TGCCACAAGCAGGAATGAG
Aggrecan	CTGCCTCAGGGATCCGTAAAG	CCTCTGCCTCAGGAATGACAT
SOX9	CCTTGAGTCCTTGCGCGGCA	TTGGCCCTCCTCCTCCAGCC
collagen I	CCGAGGGCCCACTAAAGG	GCTGTTGAAGTCACAGGAGACAA
osteopontin (OPN)	CCTGTGGCCTTGGGCCTCAA	GGTGCTGATGTACCAGTTGGG
osteonectin	ATGGACGATCTGTTTCCC	GTCTTAGTGGTATCTGTGCT

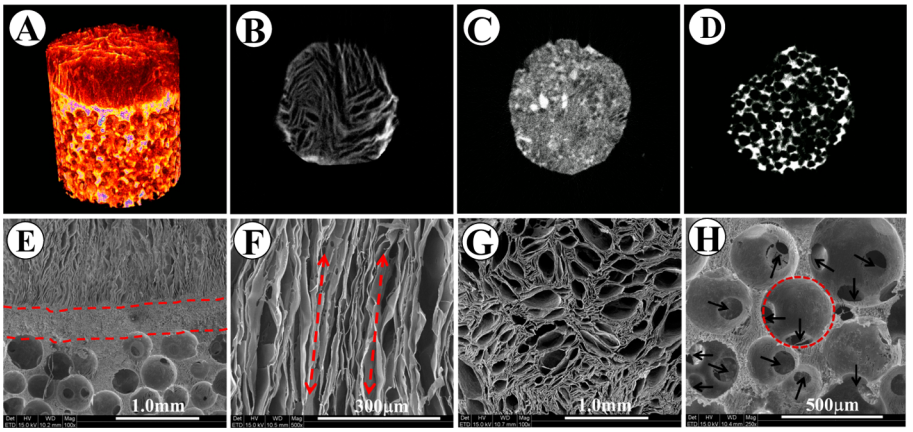

Figure 2. Gross structure and morphology of integrated osteochondral scaffold. (A–D) Micro-CT images: (A) the integrated osteochondral scaffold possessed three layers with different densities, including (B) chondral (top) layer, (C) intermediate layer (area between red dashed lines), and (D) a bony layer (bottom). (E–H) SEM images with different magnifications: (E) longitudinal section of integrated osteochondral scaffolds; (F) longitudinal section of chondral layer (arrows indicate oriented pores); (G) cross section of chondral layer; (H) cross section of bony layer (red circle indicates a macropore; arrows indicate openings between macropores).

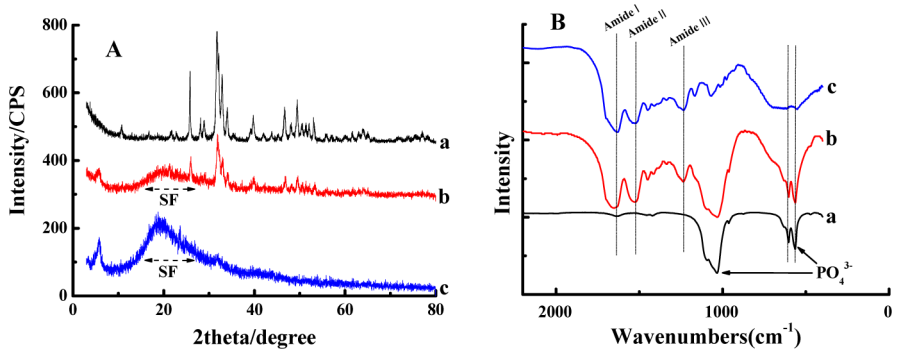

Figure 3. (A) XRD patterns and (B) FTIR spectra of integrated osteochondral scaffold: (a) pure hydroxyapatite (HA); (b) HA/SF composite in the intermediate and bony layers; and (c) pure silk fibroin (SF) in the chondral layer.

according to protocols provided by the manufacturer. Similarly, collagen type I in the bony layer was quantified by use of a rabbit collagen type I ELISA kit (Blue Gene Biotech, Shanghai).

2.9. Real-Time Polymerase Chain Reaction Assay of Cartilage- and Bone-Related Gene Expression. Chondrogenic- and osteogenic-induced ADSCs were seeded onto the chondral and bony layer, respectively, and cultured in chondrogenic or osteogenic induction medium for 7 and 21 days. At the same time, noninduced ADSCs were seeded onto chondral or bony layers and cultured in noninduced culture medium for 1 day as controls. Expression of cartilage- and bone-related genes was analyzed by RT-PCR. Briefly, the cell-scaffold samples (n = 5) were ground to a powder in a mortar and pestle filled with liquid nitrogen, and the resulting powders were immersed in TRIzol reagent (Invitrogen, Carlsbad, CA). RNA was extracted following the manufacturer's protocol. The total RNA concentration was quantified by use of a NanoDrop1000 (Thermo Scientific). Subsequently, 2 μg of total RNA was reverse-transcribed by use of a First cDNA synthesis kit (Fermentas Life Sciences, York, U.K.). RT-PCR employed the SYBR green system (Fermentas Life Sciences) at 95 °C for 10 min, followed by 40 cycles at 94 °C for 30 s, 56 °C for 60 s, and 72 °C for 40 s. Expression was calculated by the 2-ΔΔCt method and normalized to that of glyceraldehyde-3-phosphate dehydrogenase (GAPDH). Primer sequences are listed in Table 1.

2.10. Compression Testing. Compressive elastic moduli of the scaffolds (blank scaffold and 1- and 3-week culture, n = 5 per group) were measured by use of a micromaterial mechanical testing system (MTF-100, Tianjin, China). The scaffolds were immersed in PBS for 4 h and then fixed on the clamp of the testing system. A constant compression speed of 0.5 mm/min was used. Stress–strain curves were recorded by the computer software. Compressive elastic moduli were calculated from the slopes of the stress–strain curves.

2.11. Statistical Analysis. SPSS v17.0 (SPSS Inc., Chicago, IL) was used for data analysis. Data are presented as the mean ± standard deviation (SD) and compared by one-way analysis of variance (ANOVA) and the Newman-Keuls comparison test. $P < 0.05$ was considered statistically significant.

3. RESULTS

3.1. Fabrication and Characterization of Scaffolds. The gross structure and morphology of the scaffolds are shown in Figure 2. Micro-CT revealed that the integrated scaffold had a consecutively overlapping trilayer structure (Figure 2A) with different densities and pore structures, including a chondral (top) layer (Figure 2B), intermediate layer (Figure 2C), and bony (bottom) layer (Figure 2D). SEM revealed a more distinct intermediate layer between the chondral and bony layers (Figure 2E). The chondral layer had an oriented microtubularlike porous structure (Figure 2F,G), which resulted from the TIPS technique. The bony layer had an interconnected macropore structure (Figure 2H), which resulted from paraffin-sphere leaching technique. The average pore diameters of the chondral and bony layers were 112.43 ± 12.65 and 362.23 ± 26.52 μm, respectively. The porosities of the chondral and bony layers were as high as 85.30% ± 1.80% and 90.25% ± 2.05%, respectively.

Chemical components of the two layers were characterized by X-ray diffraction (XRD) patterns and Fourier transform infrared (FTIR) spectra.[38] The XRD patterns presented the typical peaks for crystalline hydroxyapatite (HA) according to the standard powder diffraction file (Figure 3A, spectrum a). The broad peak between 17° and 27° was caused by the amorphous structure of silk fibroin (SF) (Figure 3A, spectra b and c). The XRD pattern of SF/HA composite exhibited HA and SF peaks (Figure 3A, spectrum b). In the FTIR spectrum of SF/HA composite (Figure 3B, spectrum b), the peaks at 579 and 609 cm^{-1} were attributed to pure HA (Figure 3B, spectrum a), and the peaks at 1230−1250, 1520−1544, and 1630−1655 cm^{-1} corresponded to amide III (C−N stretching), amide II (N−H bend), and amide I (carbonyl stretching) of SF, respectively (Figure 3B, spectrum c). Analysis of XRD patterns and FTIR spectra indicated that a SF/HA composite scaffold was successfully fabricated.

3.2. Adhesion and Viability of Adipose-Derived Stromal Cells within Scaffolds. Adhesion and viability of ADSCs within the chondral and bony layers of integrated osteochondral scaffolds (Figure 4A) were evaluated. The ADSCs could adhere and spread well on the walls of pores in the chondral layer (Figure 4B) or bony layer (Figure 4C). Moreover, the adhered ADSCs could secrete extracellular matrix (ECM), which suggested that both chondral and bony layers had good cytocompatibility with the ADSCs and could support the attachment and growth of ADSCs. Live/dead staining after 3 days of culture revealed that there were almost no dead cells (red shows nonspecific staining of SF). Moreover, we observed a zonal region without cells (Figure 4D), which resulted from the intermediate layer preventing ADSCs from both chondral and bony layers from mixing. The ADSCs within the chondral layer could grow in the oriented microtubular direction (Figure 4E), whereas those within the bony layer could grow along the surface of the pore wall (Figure 4F). Therefore, the ADSCs could survive within both the chondral and bony layers, in which the pore structure could regulate the growth pattern of the ADSCs.

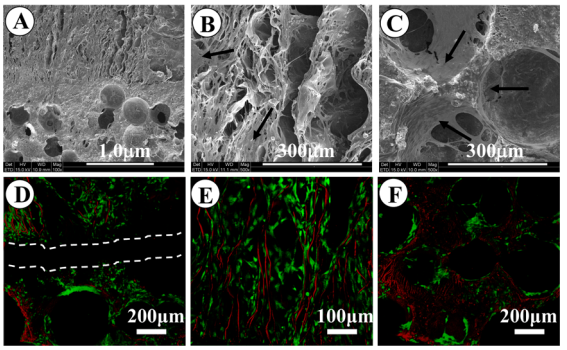

Figure 4. (A−C) Adhesion and (D−F) viability of ADSCs within the integrated osteochondral scaffold. (A) SEM images of longitudinal sections of scaffolds seeded with ADSCs after 7 days of culture, and magnified SEM images of (B) chondral layer and (C) bony layer with ADSCs (black arrows indicate ECM and cells attached to the scaffold). (D) Confocal microscopy images of live/dead staining of longitudinal sections of scaffolds seeded with ADSCs (area between white dashed lines indicates the cell-free intermediate layer), (E) chondral layer, and (F) bony layer.

3.3. Isolating Role of the Intermediate Layer. As shown in Figure 5, a cell-free region was clearly observed between the chondral layer seeded with DiO-labeled ADSCs (green) and the bony layer seeded with DiI-labeled ADSCs (red) (Figure 5A,B) after 7 days of culturing. The DiO-labeled ADSCs (green) distributed only over the chondral layer (Figure 5A−C), whereas the DiI-labeled ADSCs (red) distributed only over the bony layer (Figure 5A,B,D). These results indicated that the intermediate layer played a role in preventing the cells within chondral and bony layers from mixing with each other.

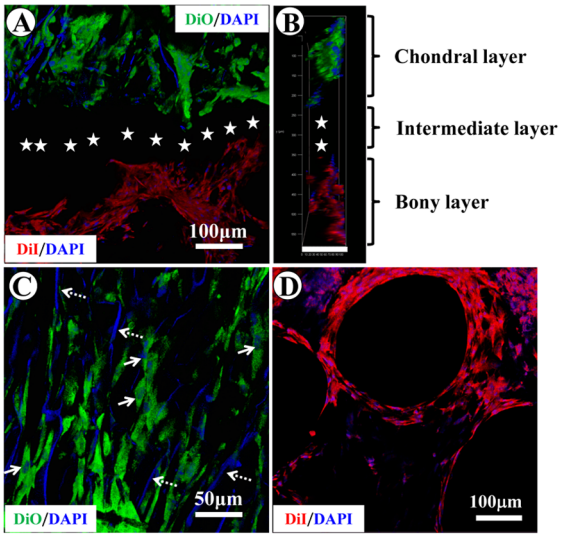

Figure 5. Isolating role of the intermediate layer. (A) Confocal microscopy image of longitudinal section of integrated osteochondral scaffold seeded with DiO-labeled ADSCs on the chondral layer and DiI-labeled ADSCs on the bony layer. (B) Profile view (scale bar 150 μm). White stars indicate the cell-free intermediate layer. Also shown are magnified images of (C) chondral layer and (D) bony layer. White solid arrows indicate cell nuclei, which were stained by DAPI; white dashed arrows indicate nonspecific staining of SF.

3.4. Cell Proliferation and Extracellular Matrix Secretion. H/E staining (Figure 6A−C) revealed that chondrogenic-induced ADSCs could infiltrate the chondral

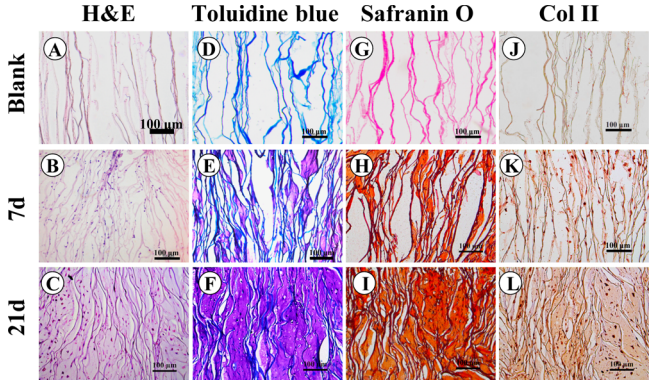

Figure 6. Histology and immunohistology of chondrogenic matrix formation within the chondral layer seeded with chondrogenic-induced ADSCs after 7 and 21 days of culturing. (A–C) H/E staining for cells; (D–F) toluidine blue staining and (G–I) safranin O staining for GAG; and (J–L) immunohistochemical staining for collagen type II.

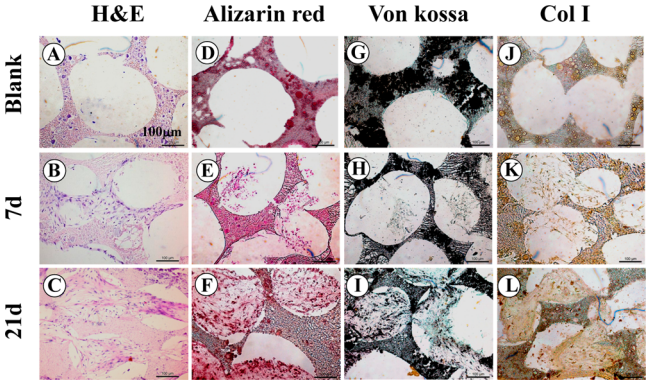

Figure 8. Histology and immunohistology of osteogenic matrix formation within the bony layer seeded with osteogenic-induced ADSCs after 7 and 21 days of culturing. (A–C) H/E staining for distribution of cells; (D–F) Alizarin red staining and (G–I) von Kossa staining for calcium deposition; and (J–L) immunohistological staining for collagen type I.

layer. The cell density continued to increase with culture time, and round chondrocyte-like cells embedded in ECM could be observed after 21 days of culture (Figure 6F,I; clearer images in Figure S1, Supporting Information). Toluidine blue staining (Figure 6D–F), safranin O staining (Figure 6G–I), and immunohistological staining (Figure 6J–L) revealed that glycosaminoglycan (GAG) and collagen type II in the chondrogenic matrix increased with culture time. Moreover, GAG and collagen type II were uniformly distributed throughout the entire chondral layer after 21 days of culture. Quantitative analysis results for cell proliferation and GAG and collagen type II within the chondral layer (Figure 7) were consistent with those of histological and immunohistological stainings (Figure 6).

On the bony layer, the seeded osteogenic-induced ADSCs could grow inside the macropores through the openings between macropores (Figure 8). As the culture time increased from 7 to 21 days, cell density within the macropores increased (Figure 8A–C). Alizarin red staining (Figure 8D–F), von Kossa staining (Figure 8G–I), and immunohistochemical staining (Figure 8J–L) revealed that the osteogenic-induced ADSCs could secrete bone matrix–calcium and collagen type I, respectively, which increased with increasing culture time. Quantitative analysis results for cell proliferation and collagen type I within bony layer (Figure 9) were consistent with those of the histological and immunohistochemical stainings (Figure 8). However, an increase in calcium deposition was not detected during quantitative analysis because there was a large amount of HA in the bony layer.

3.5. Gene Expression of Chondrogenic and Osteogenic Differentiation. The expression of chondrogenic-related genes (collagen type II, aggrecan, and SOX-9) was significantly increased with increasing culture time ($P < 0.01$) (Figure 10A–C). Compared with noninduced ADSCs, which

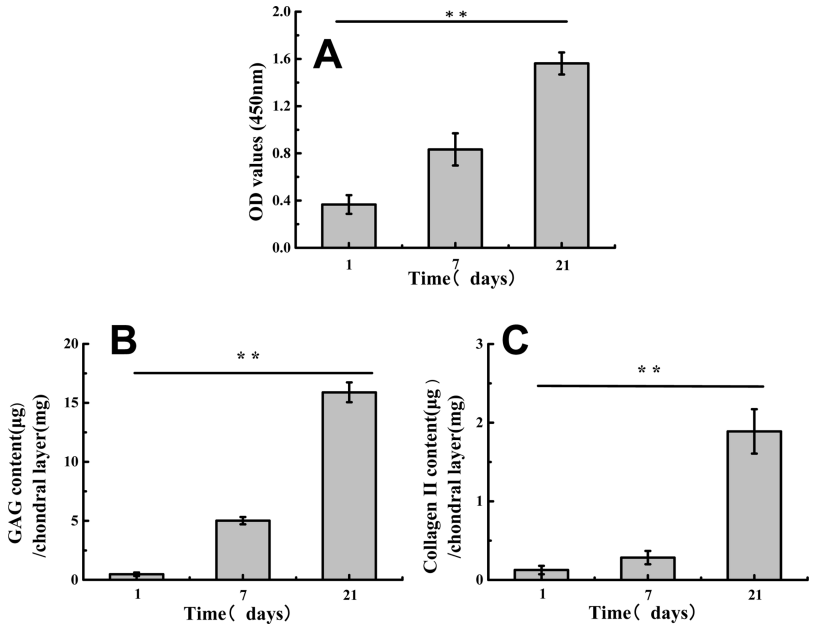

Figure 7. Quantitative analysis of (A) cell proliferation, (B) GAG content, and (C) collagen II content within the chondral layer seeded with chondrogenic-induced ADSCs after 1, 7, and 21 days of culturing. $^{**}P < 0.01$. Data are given as mean ± SD, $n = 5$.

dx.doi.org/10.1021/am5036708 | ACS Appl. Mater. Interfaces 2014, 6, 16696–16705

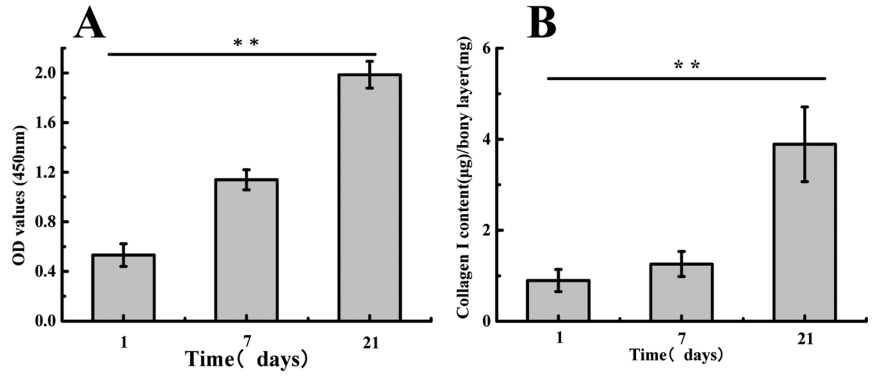

Figure 9. Quantitative analysis of (A) cell proliferation and (B) secretion of collagen I within the bony layer seeded with osteogenic-induced ADSCs after culturing for 1, 7, and 21 days of culturing. $^{**}P < 0.01$. Data are given as mean ± SD, $n = 5$.

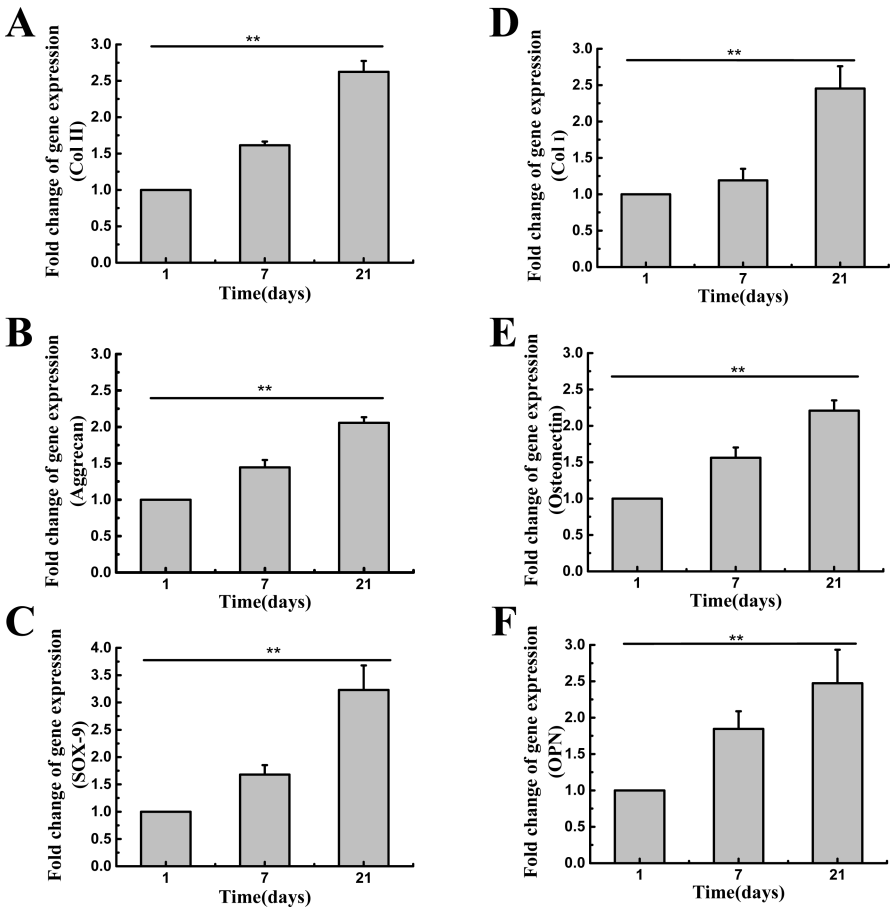

Figure 10. (A–C) Expression profiles of chondrogenic-related genes of (A) collagen type II, (B) aggrecan, and (C) SOX-9 within the chondral layer. (D–F) Expression profiles of osteogenic-related genes of (D) collagen type I, (E) osteonectin, and (F) osteopontin (OPN) within the bony layer after 7 and 21 days of culturing. $^{**}P < 0.01$. Data are given as mean ± SD, $n = 5$.

were cultured for 1 day in non-chondrogenic-induced culture medium, the expression levels of collagen type II, aggrecan, and SOX-9 genes were all up-regulated at day 7. The levels of gene expression were all increased significantly ($P < 0.01$) at day 21, which suggested that the chondrogenic-induced ADSCs could differentiate toward chondrocytes within the chondral layer. On the other hand, expression levels of osteogenic-related genes [collagen type I, osteopontin (OPN), and osteonectin] (Figure 10D–F) were all upregulated at 21 days ($P < 0.01$).

3.6. Compressive Elastic Modulus. The compressive elastic modulus of the chondral layer significantly increased from 52.48 ± 5.78 kPa for the blank scaffold to 84.41 ± 7.12 kPa after 21 days of culturimg ($P < 0.05$) (Figure 11A). The mean compressive elastic modulus of the bony layer significantly increased from 54.93 ± 5.44 kPa for the blank scaffold to 109.91 ± 10.02 kPa after 21 days of culturing ($P < 0.05$) (Figure 11B).

4. DISCUSSION

Osteochondral tissue engineering involves cartilage and subchondral bone, which have significant differences in biological structure, composition, and mechanical properties.

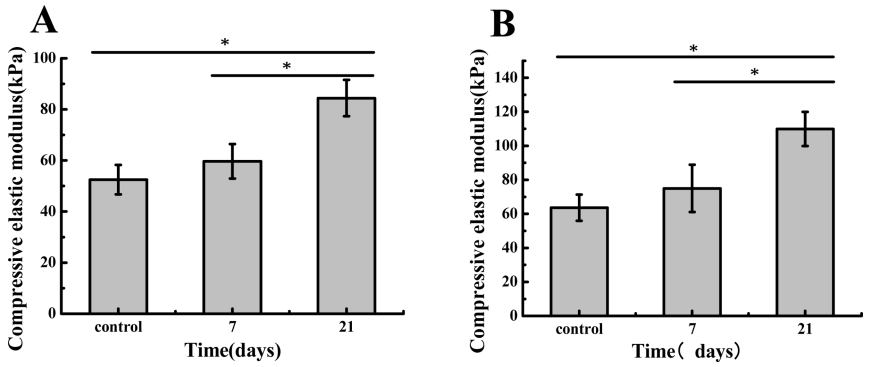

Figure 11. Compressive elastic modulus of (A) chondral layer seeded with chondrogenic-induced ADSCs and (B) bony layer seeded with osteogenic-induced ADSCs after 7 and 21 days of culturing. *$P < 0.05$. Data are given as mean ± SD, $n = 5$.

To date, natural and synthetic polymers, inorganic materials, and their composites have been used to fabricate osteochondral scaffolds that mimic different regions of native osteochondral tissue.[32,39] Silk is a promising biomaterial that has attracted considerable attention for cartilage and subchondral bone. Hydrophilic SF materials can load growth factors to create a specific endogenous niche to promote the seeded stem cells to differentiate into chondrocytes and osteoblasts in vitro and in vivo.[37] However, integrated silk scaffolds with different porous structures have not been investigated for the simultaneous regeneration of cartilage and subchondral bone. Fabricating this type of integrated silk osteochondral scaffold with an interface is still a challenge. In this study, we aimed to develop a method for fabricating an integrated silk osteochondral scaffold with a favorable environment for the adhesion, proliferation, and differentiation of ADSCs.

To repair the bony region of osteochondral tissue, a 3D porous structure is generally adopted as a scaffold, which is commonly prepared by freeze-drying and salt-particle leaching.[1,5,6] Compared to these methods, the paraffin-microsphere leaching method has more advantages for controlling the size and interconnectivity of pores by selecting paraffin microspheres with different sizes as porogens and by adjusting the heating time and temperature. Ma and co-workers[40] first developed and used this method to prepare a PLGA porous scaffold, but few reports have used this method to prepare SF scaffolds. On the basis of our previous experience,[41] in this study we mimicked the composition of native bone and successfully fabricated a porous SF/HA structure as a bone scaffold through the use of paraffin-microsphere leaching. The key to this process is determining the concentrations of SF and HA. For filling the paraffin-microsphere assembly, if the concentration is too low, the resulting scaffolds are very weak and are easily broken. In practice, we adopted a 10% SF and HA mixture with an equivalent weight ratio, which could be forced into the paraffin-microsphere assembly under vacuum (Figure 1). The intermediate layer could be created by leaving a small amount of the above mixture on the top of the paraffin-microsphere assembly, through which the intermediate layer could be well bonded to the lower layer (bony layer). The thickness of the intermediate layer could be regulated by the amount of the remaining mixture.

The deep zone of normal articular cartilage tissue consists of longitudinally oriented chondrocytes and cartilage matrix, and it plays the most important role in distributing load and resisting compression. Because the deep zone is the largest part of articular cartilage,[42] the cartilage region of the osteochondral scaffold is designed as a longitudinally oriented structure that mimics the deep zone of articular cartilage. Zhou and co-workers[43] demonstrated that oriented scaffolds could better regulate the distribution, alignment, and migration of MSCs or chondrocytes than nonoriented scaffolds. Modified temperature gradient-guided TIPS is an effective method for preparing this type of oriented scaffold. PLGA,[43] chitosan,[44] gelatin,[45] and SF[46] oriented scaffolds have been successfully prepared by use of modified temperature gradient-guided TIPS and have been used for cartilage engineering. However, the use of an oriented SF structure for cartilage scaffolds in integrated osteochondral scaffolds has not been reported. In this study, we prepared a layer of oriented SF scaffolds on the intermediate layer via modified temperature gradient-guided TIPS. To allow the oriented SF structure to tightly bond with the intermediate layer, the frozen intermediate layer was slightly melted such that the added SF solution could slightly immerse into the intermediate layer. The oriented SF structure and macroporous structure were connected together through the intermediate layer to create an integrated osteochondral scaffold that contained three distinct layers (Figure 2).

For large 3D scaffolds, the attachment, proliferation, and especially the infiltration of cells inside scaffolds are necessary. Although we used ethanol, *n*-hexane, and other chemical reagents during the preparation, the ADSCs still had good adhesion and proliferation on the chondral and bony layers. The ADSCs could survive well in the two layers (Figure 4). These results fully demonstrated that the integrated osteochondral scaffolds exhibit good biocompatibility and no cytotoxicity. Additionally, the seeded ADSCs could infiltrate the chondral and bony layers with different distribution patterns. The ADSCs showed an oriented distribution due to the guidance by oriented pores in the chondral layer, which is beneficial for the formation of oriented chondrocytes and cartilage matrix. In the bony layer, the ADSCs were distributed uniformly inside the pores, which would favor the formation of uniform bone tissue. More importantly, the existence of an intermediate layer prevented the ADSCs in chondral and bony layers from mixing with each other (Figures 4D and 5A,B). Therefore, the intermediate layer played an efficient role in creating a relatively independent microenvironment for regenerating cartilage and bone.

The simultaneous differentiation of ADSCs toward chondrocytes and osteoblasts on the same integrated scaffolds is not easy because different inductive factors need to be used,[47] particularly in vitro. To further investigate the potential of ADSCs differentiating toward cartilage and bone in the

chondral and bony layers, we proposed that the microenvironments of the separated chondral and bony layers were similar to those of the integrated scaffolds. We seeded the induced ADSCs on separated chondral and bony layers and cultured them in different culture media containing chondrogenic and osteogenic induction factors, respectively. For the ADSC-seeded chondral layer, chondrocyte-like cells surrounded by ECM rich in GAG and collagen type II were observed (Figure 6; Figure S1, Supporting Information), and the cartilage-related matrix—GAG and collagen type II content increased over the culture time of 21 days (Figures 6 and 7). The expression levels of chondrogenic-related genes within the chondral layer were also upregulated over the culture time. Taken together, these findings strongly suggest that the chondral layer supports the chondrogenesis of the ADSCs under chondrogenic conditions (with TGF-b1 and IGF). Similarly, in the ADSC-seeded bone layer, the expressions of osteogenic-related genes and bone-related matrix content (calcium and collagen type I) were increased with culture time (Figures 8 and 9), indicating that the bony layer supports osteogenic differentiation of the ADSCs under osteogenic conditions (with dexamethasone). Consequently, the pores were filled with increasingly more cartilage-related and bone matrix as the culture time increased, resulting in an increase in the compressive elastic modulus (Figure 11).

The present results show a promising prospect for the use of novel 3D integrated SF scaffolds in osteochondral tissue engineering in vitro. However, whether ADSCs can differentiate into cartilage and bone in the corresponding chondral and bony layers of integrated scaffolds needs to be further investigated through in vivo implantation. Furthermore, the isolating role of the intermediate layer needs to be confirmed in vivo.

5. CONCLUSIONS

A biomimetic integrated trilayered osteochondral scaffold consisting of SF/HA is successfully fabricated by combining paraffin-microsphere leaching with the modified temperature gradient-guided TIPS technique. This scaffold exhibits good biocompatibility for supporting ADSC growth, infiltration, ECM secretion, and differentiation toward chondrocytes and osteoblasts in vitro. Specifically, the intermediate layer can play a role in preventing the cells within the chondral and the bony layers from mixing with each other. These findings indicate that our prepared trilayered SF scaffolds are versatile candidates for repairing osteochondral defects. Further studies will focus on the regeneration of OC defects in animal models.

■ ASSOCIATED CONTENT

Supporting Information

Additional text with details of materials; two figures showing results of flow cytometry for characterization of ADSCs and enlarged images of chondrocyte morphology in Figure 5F,I. This material is available free of charge via the Internet at http://pubs.acs.org.

■ AUTHOR INFORMATION

Corresponding Authors

*E-mail wly@nankai.edu.cn.
*E-mail yangqiang1980@126.com.

Author Contributions

⊥X.D. and M.Z. contributed equally to this work.

Notes

The authors declare no competing financial interest.

■ ACKNOWLEDGMENTS

This study was supported by the National Natural Science Foundation of China (31300798, 81272046 and 31470937), National Program on Key Basic Research Project (973 Program, 2011CB606202), and Program for Changjiang Scholars and Innovative Research Team in University (IRT13023).

■ REFERENCES

(1) Nooeaid, P.; Salih, V.; Beier, J. P.; Boccaccini, A. R. Osteochondral Tissue Engineering: Scaffolds, Stem Cells and Applications. *J. Cell. Mol. Med.* **2012**, *16*, 2247−2270.
(2) Cengiz, I. F.; Oliveira, J. M.; Reis, R. L. Tissue Engineering and Regenerative Medicine Strategies for the Treatment of Osteochondral Lesions. In *3D Multiscale Physiological Human*; Thalmann, N. M., Ratib, O., Choi, H. F., Eds.; Springer Press: London, 2014; pp 25−47.
(3) Hunziker, E. Articular Cartilage Repair: Basic Science and Clinical Progress, a Review of the Current Status and Prospects. *Osteoarthritis Cartilage* **2002**, *10*, 432−463.
(4) Spalazzi, J. P.; Doty, S. B.; Moffat, K. L.; et al. Development of Controlled Matrix Heterogeneity on a Triphasic Scaffold for Orthopedic Interface Tissue Engineering. *Tissue Eng.* **2006**, *12*, 3497−3508.
(5) Nukavarapu, S. P.; Dorcemus, D. L. Osteochondral Tissue Engineering: Current Strategies and Challenges. *Biotechnol. Adv.* **2013**, *31*, 706−721.
(6) Shimomura, K.; Moriguchi, Y.; Murawski, C. D.; Yoshikawa, H.; Nakamura, N. Osteochondral Tissue Engineering with Biphasic Scaffold: Current Strategies and Techniques. *Tissue Eng., Part B* **2014**, DOI: 10.1089/ten.teb.2013.0543.
(7) Panseri, S.; Russo, A.; Cunha, C.; Bondi, A.; Di Martino, A.; Patella, S.; et al. Osteochondral Tissue Engineering Approaches for Articular Cartilage and Subchondral Bone Regeneration. *Knee Surg. Sports Traumatol. Arthrosc.* **2012**, *20*, 1182−1191.
(8) Chen, J.; Chen, H.; Li, P.; Diao, H.; Zhu, S.; Dong, L.; et al. Simultaneous Regeneration of Articular Cartilage and Subchondral Bone in Vivo Using MSCs Induced by a Spatially Controlled Gene Delivery System in Bilayered Integrated Scaffolds. *Biomaterials* **2011**, *32*, 4793−4805.
(9) Da, H.; Jia, S. J.; Meng, G. L.; Cheng, J. H.; Zhou, W.; Xiong, Z.; et al. The Impact of Compact Layer in Biphasic Scaffold on Osteochondral Tissue Engineering. *PLoS One* **2013**, *8*, No. e54838.
(10) O'Shea, T. M.; Miao, X. Bilayered Scaffolds for Osteochondral Tissue Engineering. *Tissue Eng., Part B* **2008**, *14*, 447−464.
(11) Hoemann, C.; Lafantaisie-Favreau, C. H.; Lascau-Coman, V.; Chen, G.; Guzmán-Morales, J. The Cartilage-Bone Interface. *J. Knee Surg.* **2012**, *25*, 85−98.
(12) Bullough, P. G.; Jagannath, A. The Morphology of the Calcification Front in Articular Cartilage. Its Significance in Joint Function. *J. Bone Joint Surg. Br.* **1983**, *65*, 72−78.
(13) Oegema, T. R.; Carpenter, R. J.; Hofmeister, F.; et al. The Interaction of the Zone of Calcified Cartilage and Subchondral Bone in Osteoarthritis. *Microsc. Res. Technol.* **1997**, *37*, 324−332.
(14) Hunziker, E. B.; Driesang, I. M. K.; Saager, C. Structural Barrier Principle for Growth Factor-based Articular Cartilage Repair. *Clin. Orthop. Relat. Res.* **2001**, 182−189.
(15) Nooeaid, P.; Roether, J. A.; Weber, E.; Schubert, D. W.; Boccaccini, A. R. Technologies for Multilayered Scaffolds Suitable for Interface Tissue Engineering. *Adv. Eng. Mater.* **2014**, *16*, 319−327.
(16) Jeon, J. E.; Vaquette, C.; Klein, T. J.; Hutmacher, D. W. Perspectives in Multiphasic Osteochondral Tissue Engineering. *Anat. Rec.* **2014**, *297*, 26−35.
(17) Benya, P. D.; Shaffer, J. D. Dedifferentiated Chondrocytes Express the Differentiated Collagen Phenotype When Cultured in Agarose Gels. *Cell* **1982**, *30*, 215−224.

(18) Schnabel, M. Dedifferentiation-associated Changes in Morphology and Gene Expression in Primary Human Articular Chondrocytes in Cell Culture. *Osteoarthritis Cartilage* **2002**, *10*, 62−70.
(19) Wang, Y. Z.; Kim, H. J.; Vunjak-Novakovic, G.; Kaplan, D. L. Stem Cell-based Tissue Engineering with Silk Biomaterials. *Biomaterials* **2006**, *27*, 6064−6082.
(20) Sundelacruz, S.; Kaplan, D. L. Stem Cell- and Scaffold-based Tissue Engineering Approaches to Osteochondral Regenerative Medicine. *Semin. Cell. Dev. Biol.* **2009**, *20*, 646−655.
(21) Correia, C.; Bhumiratana, S.; Yan, L. P.; Oliveira, A. L.; Gimble, J. M.; Rockwood, D.; et al. Development of Silk-based Scaffolds for Tissue Engineering of Bone from Human Adipose-derived Stem Cells. *Acta Biomater.* **2012**, *8*, 2483−2492.
(22) Zanetti, A. S.; Sabliov, C.; Gimble, J. M.; Hayes, D. J. Human Adipose-derived Stem Cells and Three-dimensional Scaffold Constructs: A Review of the Biomaterials and Models Currently Used for Bone Regeneration. *J. Biomed. Mater. Res., Part B* **2013**, *101B*, 187−199.
(23) Estes, B. T.; Diekman, B. O.; Gimble, J. M.; Guilak, F. Isolation of Adipose-derived Stem Cells and Their Induction to a Chondrogenic Phenotype. *Nat. Protoc.* **2010**, *5*, 1294−1311.
(24) Bunnell, B.; Flaat, M.; Gagliardi, C.; Patel, B.; Ripoll, C. Adipose-derived Stem Cells: Isolation, Expansion and Differentiation. *Methods* **2008**, *45*, 115−120.
(25) Zuk, P. Adipose-derived Stem Cells in Tissue Regeneration: A Review. *ISRN Stem Cells* **2013**, *2013*, 1−35.
(26) Gimble, J. M.; Katz, A. J.; Bunnell, B. A. Adipose-derived Stem Cells for Regenerative Medicine. *Circ. Res.* **2007**, *100*, 1249−1260.
(27) Kasoju, N.; Bora, U. Silk Fibroin in Tissue Engineering. *Adv. Health Mater.* **2012**, *1*, 393−412.
(28) Vepari, C.; Kaplan, D. L. Silk as a Biomaterial. *Prog. Polym. Sci.* **2007**, *32*, 991−1007.
(29) Hofmann, S.; Knecht, S.; Langer, R.; Kaplan, D. L.; Vunjak-Novakovic, G.; Merkle, H. P.; et al. Cartilage-like Tissue Engineering Using Silk Scaffolds and Mesenchymal Stem Cells. *Tissue Eng.* **2006**, *12*, 2729−2738.
(30) Wang, Y. Z.; Kim, U. J.; Blasioli, D. J.; Kim, H. J.; Kaplan, D. L. In vitro Cartilage Tissue Engineering with 3D Porous Aqueous-derived Silk Scaffolds and Mesenchymal Stem Cells. *Biomaterials* **2005**, *26*, 7082−7094.
(31) Wang, Y. Z.; Blasioli, D. J.; Kim, H. J.; Kim, H. S.; Kaplan, D. L. Cartilage Tissue Engineering with Silk Scaffolds and Human Articular Chondrocytes. *Biomaterials* **2006**, *27*, 4434−4442.
(32) Rezwan, K.; Chen, Q. Z.; Blaker, J. J.; Boccaccini, A. R. Biodegradable and Bioactive Porous Polymer/Inorganic Composite Scaffolds for Bone Tissue Engineering. *Biomaterials* **2006**, *27*, 3413−3431.
(33) Danilchenko, S. N.; Kalinkevich, O. V.; Pogorelov, M. V.; et al. Chitosan−Hydroxyapatite Composite Biomaterials Made by a One Step Co-precipitation Method: Preparation, Characterization and in Vivo. *J. Biol. Phys. Chem.* **2009**, *9*, 119−126.
(34) Zhou, J.; Xu, C.; Wu, G.; Cao, X.; Zhang, L.; Zhai, Z.; et al. In Vitro Generation of Osteochondral Differentiation of Human Marrow Mesenchymal Stem Cells in Novel Collagen−Hydroxyapatite Layered Scaffolds. *Acta Biomater.* **2011**, *7*, 3999−4006.
(35) Bhumiratana, S.; Grayson, W. L.; Castaneda, A.; Rockwood, D. N.; Gil, E. S.; Kaplan, D. L.; et al. Nucleation and Growth of Mineralized Bone Matrix on Silk-Hydroxyapatite Composite Scaffolds. *Biomaterials* **2011**, *32*, 2812−2820.
(36) Zhu, M.; Wang, K.; Mei, J.; Li, C.; Zhang, J.; Zheng, W.; et al. Fabrication of Highly Interconnected Porous Silk Fibroin Scaffolds for Potential Use as Vascular Grafts. *Acta Biomater.* **2014**, *10*, 2014−2023.
(37) Saha, S.; Kundu, B.; Kirkham, J.; Wood, D.; Kundu, S. C.; Yang, X. B. B. Osteochondral Tissue Engineering In Vivo: A Comparative Study Using Layered Silk Fibroin Scaffolds from Mulberry and Nonmulberry Silkworms. *PLoS One* **2013**, *8*, No. e80004.
(38) Zhang, W.; Chen, J.; Tao, J.; Hu, C.; Chen, L.; Zhao, H.; et al. The Promotion of Osteochondral Repair by Combined Intra-articular Injection of Parathyroid Hormone-related Protein and Implantation of a Bi-layer Collagen-silk Scaffold. *Biomaterials* **2013**, *34*, 6046−6057.
(39) Puppi, D.; Chiellini, F.; Piras, A. M.; Chiellini, E. Polymeric Materials for Bone and Cartilage Repair. *Prog. Polym. Sci.* **2010**, *35*, 403−440.
(40) Smith, I. O.; Liu, X. H.; Smith, L. A.; Ma, P. X. Nanostructured Polymer Scaffolds for Tissue Engineering and Regenerative Medicine. *Wiley Interdiscip. Rev.: Nanomed. Nanobiotechnol.* **2009**, *1*, 226−236.
(41) Zeng, C.; Yang, Q.; Zhu, M. F.; Du, L. L.; Zhang, J. M.; Ma, X. L.; et al. Silk Fibroin Porous Scaffolds for Nucleus Pulposus Tissue Engineering. *Mater. Sci. Eng. C* **2014**, *37*, 232−240.
(42) Wong, M.; Carter, D. R. Articular Cartilage Functional Histomorphology and Mechanobiology: A Research Perspective. *Bone* **2003**, *33*, 1−13.
(43) Zhang, Y.; Yang, F.; Liu, K.; Shen, H.; Zhu, Y.; Zhang, W.; Liu, W.; Wang, S.; Cao, Y.; Zhou, G. The Impact of PLGA Scaffold Orientation on in Vitro Cartilage Regeneration. *Biomaterials* **2012**, *33*, 2926−2935.
(44) Wen, P.; Gao, J. P.; Zhang, Y. L.; Li, X. L.; Long, Y.; Wu, X. H.; et al. Fabrication of Chitosan Scaffolds with Tunable Porous Orientation Structure for Tissue Engineering. *J. Biomater. Sci., Polym. Ed.* **2011**, *22*, 19−40.
(45) Wu, X.; Liu, Y.; Li, X.; Wen, P.; Zhang, Y.; Long, Y.; et al. Preparation of Aligned Porous Gelatin Scaffolds by Unidirectional Freeze-drying Method. *Acta Biomater.* **2010**, *6*, 1167−1177.
(46) Oliveira, A. L.; Sun, L.; Kim, H. J.; Hu, X.; Rice, W.; Kluge, J.; et al. Aligned Silk-Based 3-D Architectures for Contact Guidance in Tissue Engineering. *Acta Biomater.* **2012**, *8*, 1530−1542.
(47) Wendt, D.; Jakob, M.; Martin, I. Bioreactor-based Engineering of Osteochondral Grafts: From Model Systems to Tissue Manufacturing. *J. Biosci. Bioeng.* **2005**, *100*, 489−494.